ACS APPLIED POLYMER MATERIALS

pubs.acs.org/acsapm Article

Mechanical Recycling of 3D-Printed Thermosets for Reuse in Vat Photopolymerization

Erin M. Maines, Michaela A. Polley, Greg Haugstad, Brenda Zhao, Theresa M. Reineke,* and Christopher J. Ellison*

Cite This: *ACS Appl. Polym. Mater.* 2024, 6, 4625−4633 Read Online

ACCESS | Metrics & More | Article Recommendations | Supporting Information

ABSTRACT: Additive manufacturing, otherwise known as three-dimensional (3D) printing, is a rapidly growing technique that is increasingly used for the production of polymer products, resulting in an associated increase in plastic waste generation. Waste from a particular class of 3D-printing, known as vat photopolymerization, is of particular concern, as these materials are typically thermosets that cannot be recycled or reused. Here, we report a mechanical recycling process that uses cryomilling to generate a thermoset powder from photocured parts that can be recycled back into the neat liquid monomer resin. Mechanical recycling with three different materials is demonstrated: two commercial resins with characteristic brittle and elastic mechanical properties and a third model material formulated in-house. Studies using photocured films showed that up to 30 wt% of the model material could be recycled producing a toughness of 2.01 ± 0.55 MJ/m^3, within error of neat analogues (1.65 ± 0.27 MJ/m^3). Using dynamic mechanical analysis and atomic force microscopy-based infrared spectroscopy, it was determined that monomers diffuse into the recycled powder particles, creating interpenetrating networks upon ultraviolet (UV) exposure. This process mechanically adheres the particles to the matrix, preventing them from acting as failure sites under a tensile load. Finally, 3D-printing of the commercial brittle material with 10 wt% recycle content produced high quality parts that were visually similar. The maximum stress (46.7 ± 6.2 MPa) and strain at break (11.6 ± 2.3%) of 3D-printed parts with recycle content were within error the same as neat analogues (52.0 ± 1.7 MPa; 13.4 ± 1.8%). Overall, this work demonstrates mechanical recycling of photopolymerized thermosets and shows promise for the reuse of photopolymerized 3D-printing waste.

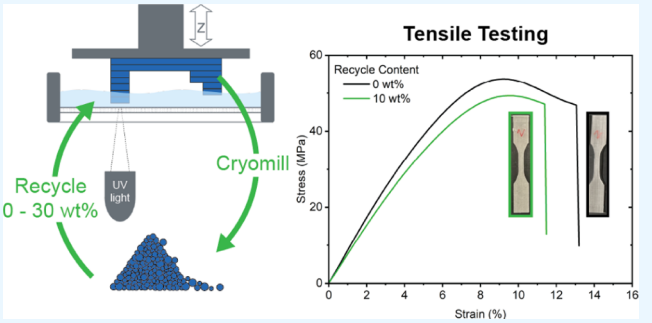

KEYWORDS: *3D-printing, mechanical recycling, cryomilling, thermosets, vat photopolymerization*

1. INTRODUCTION

Additive manufacturing (also known as three-dimensional (3D) printing) is rapidly growing and continuously expanding beyond prototyping applications toward commercial production.[1,2] These processes utilize many materials, with high-performance polymers being of particular interest because of their durability, ease of use, and versatility.[2] As 3D-printing has an annual growth rate of >10%,[1,2] its contribution to the total amount of plastic waste is also increasing. It has been estimated that between 1950 and 2017, over 5000 million metric tons of plastic waste has been generated, which has mostly ended up in landfills or the environment.[3] To mitigate the growing role of 3D-printing in the plastic waste crisis, more sustainable solutions involving recycling and other approaches are needed.

Vat photopolymerization is an essential 3D-printing technology because it can readily form parts from thermally and chemically stable materials, known as thermosets. This approach offers better feature resolution than other 3D-printing techniques, such as fused deposition modeling (FDM) that passes a thermoplastic filament through a heated nozzle, depositing a polymer melt that solidifies on a build plate. Intuitively, thermoplastics can be easily reprocessed by reheating during recycling.[4,5] In contrast, thermoset materials produced in vat photopolymerization are typically not reprocessable/recyclable or degradable,[6,7] so they usually end up in landfills and directly contribute to the plastic waste problem.

Several studies have explored methods to improve the sustainability of vat photopolymerizable materials through biobased monomers, incorporation of degradable chemistries, and reprocessable/recyclable materials.[6,8,9] As an example, covalent adaptable networks (CANs) allow for the reprocessing of thermoset materials by incorporating exchanging

Received: January 17, 2024
Revised: February 29, 2024
Accepted: March 13, 2024
Published: April 8, 2024

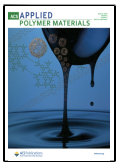

https://doi.org/10.1021/acsapm.4c00184
ACS Appl. Polym. Mater. 2024, 6, 4625−4633

chemical bonds that can be activated by heat or other means. CANs for vat photopolymerization have incorporated transesterification,[10−14] thioester-anhydride reactions,[15] Diels−Alder chemistry,[16] and other bond exchange chemistries[17−19] for recycling. Besides requiring implementation of specialized chemistries, another disadvantage to most CANs is that their reprocessability is usually limited to thermal remolding.[10−12,14−16,19] Therefore, CANs cannot be directly reused in 3D-printing applications without the use of more complex postprocessing, like a postcure heating step, to activate transesterification to reincorporate recycled materials[20] or soaking printed materials in excess small-molecule precursors to refunctionalize the system prior to a second printing.[13] While both methods maintain the chemical resistance of thermosets, the postprinting thermal and/or chemical treatment is not desirable. In other work, specially designed resin systems employing hindered urea bonds have been shown to exchange upon ultraviolet (UV) curing due to the heat of reaction during the 3D-printing process.[18] Another potential limitation of CANs is that they typically have lower thermal resistance than traditional thermosets as the dynamic bonds are activated by heat, preventing them from being used at temperatures near to or higher than the exchange temperature, typically <200 °C.[10−12,14−16,19]

In this work, a mechanical recycling approach was developed to reprocess vat photopolymerized thermoset materials such that they could be directly reprinted with neat resins. We studied three different resins: a model resin formulated in-house along with two commercial resins (Formlabs Clear and Formlabs Elastic 50A). Each of these materials was light-cured and milled into a powder using a mechanical recycling technique known as cryomilling and then recycled by physically mixing the powder into neat liquid resin. The tensile, visual, rheological, and morphological properties were evaluated in films as a function of recycle content. Building from the film studies, stereolithography (SLA) 3D-printing of the Formlabs Clear resin with and without 10 wt% recycle content was demonstrated. These findings illustrate a straightforward solvent-free process for recycling 3D-printed thermosets, enabling a more circular economy.

2. MATERIALS AND METHODS

2.1. Materials. Two commercial resins were obtained from Formlabs, Clear Resin (RS-F2-GPCL-04) and Elastic 50A Resin (RS-F2-ELCL-01) and were used as received. Three different batches of Formlabs Clear Resin were used throughout this paper. Batch-to-batch variations in the mechanical property values were observed. Quantitative comparisons were made between samples from the same batch, while qualitative trends did not vary between batches. Additional details regarding batch-to-batch variations are provided in the Supporting Information, and Table S1. Isobornyl acrylate was obtained from TCI Chemicals and was used as received. Poly(ethylene glycol diacrylate) (M_n = 575 Da) and isopropyl alcohol (ACS reagent, ≥99.5%) were obtained from Sigma-Aldrich and used as received. The photoinitiator, Omnirad 2100, was provided by IGM Resins and used as received.

2.2. Model Resin Formulation. A model resin was developed to better understand the components contributing to the recyclability. The model resin was designed as a mixture of a high T_g monofunctional acrylate and low T_g difunctional acrylate to give a network with mechanical properties that were easy to measure at room temperature. This resin is a mixture of 49.5% isobornyl acrylate, 49.5% poly(ethylene glycol) (PEG) diacrylate, and 1% photoinitiator (Omnirad 2100) by weight. As these are all liquids, the solution was vortexed until a homogeneous solution was obtained.

2.3. Cryomilling. CryoMill from Retsch equipped with liquid nitrogen cooling was used for reducing thermoset samples to powders. Samples were placed in a stainless-steel chamber with stainless-steel milling media. Two different setups were used: a 5 mL chamber with two 7 mm milling balls and a 50 mL chamber with one 25 mm milling ball. The samples were precooled with liquid nitrogen using the autoprecooling setting while shaking gently at 5 Hz to equilibrate the sample while cooling. Once the precooling was completed, the milling cycle automatically started. A milling cycle consisted of a 2 min milling period at 30 Hz and a 30 s intermediate cooling step at 5 Hz to remove any heat generated during milling. This milling cycle was then repeated for 2−8 cycles. An in-depth powder particle size study was conducted to determine the effects of particle size on the mechanical properties; this is discussed further in the Supporting Information, Figures S1−S3 and Table S2. From this study, it was found that particle sizes greater than 100 μm resulted in poor mechanical properties. Therefore, eight milling cycles, achieving an average particle size of around 70 μm, were chosen as the standard for all subsequent studies, unless indicated otherwise.

2.4. Recycled Material Formulations. For resins containing recycled powder, the liquid resin and the milled particles were weighed separately and combined to target the desired amount of recycle content. The samples were hand stirred with a plastic spatula and allowed to equilibrate for 24 h before exposure to UV light in the course of forming films or 3D-printed parts. An equilibration study (also referred to as a monomer diffusion time study) was conducted with all materials, and further details can be found in the Supporting Information.

2.5. Film Preparation for Tensile Testing and Dynamic Mechanical Analysis (DMA). Thermoset films were prepared by placing the liquid resin with or without recycle content between two glass slides with 0.5 mm Teflon spacers. The glass slides were clamped together with binder clips. The confined resin was exposed to UV light (OmniCure S1500) at 100 mW/cm^2 for 300 s. The sample was separated from the slides. For brittle materials (Clear resin), the samples were cut into rectangles (32 mm long and 6 mm wide) for tensile testing. For the elastic resin, a dumbbell cutter was used with a gauge width of 5 mm and a gauge length of 22 mm. For the model material, a dumbbell silicone mold (gauge dimensions: 3 mm × 9 mm × 0.9 mm, $W \times L \times T$) was used with a glass slide placed on top prior to UV exposure to create materials for tensile testing. For dynamic mechanical analysis, all samples were cured between glass slides and cut into rectangles with a razor blade to 20 mm long and 3 mm wide. Post UV exposure, all samples were solid throughout the entire thickness, indicating full cure. To further confirm this, gel fraction studies were conducted on the model materials, showing a high gel fraction (95.8 ± 2.7%) with little monomer remaining. Gel fraction studies on the clear and elastic resin materials were conducted also showing high gel fractions of 96.6 ± 0.4% and 96.0 ± 0.1%, respectively.

2.6. Microtome/Cryomicrotome. For the model resin, cross-sectional slices were prepared by using room-temperature microtoming. A cryomicrotome was used to create cross sections of the clear resin with 30 wt% elastic particles and the elastic resin with 30 wt% clear particles by cooling the samples to below their glass transition temperature before cutting. For both, a Leica U6 Ultramicrotome was used with or without liquid nitrogen cooling. All cut samples were prepared to around 400 nm thickness by using a glass knife and transferred to a silicon wafer for atomic force microscopy-based infrared spectroscopy (AFM-IR) measurements.

2.7. SLA 3D-Printing. For 3D-printing studies, a Formlabs Form 1+ printer was used on the Clear Resin V4 setting with a layer thickness of 200 or 50 μm. Printed parts were washed with isopropyl alcohol for 20 min (17 min soak and 3 min shaken). After drying for 1 h, the samples were postcured with UV light (OmniCure S1500) at 100 mW/cm^2. The brick and "M" prints were cured for 300 s total. The 3D-printed tensile bars were cured for 450 s on one side and then flipped and cured for an additional 450 s to ensure full cure throughout the tensile bar. Full cure was verified through tensile testing by comparing mechanical properties to those of the analogous

https://doi.org/10.1021/acsapm.4c00184
ACS Appl. Polym. Mater. 2024, 6, 4625−4633

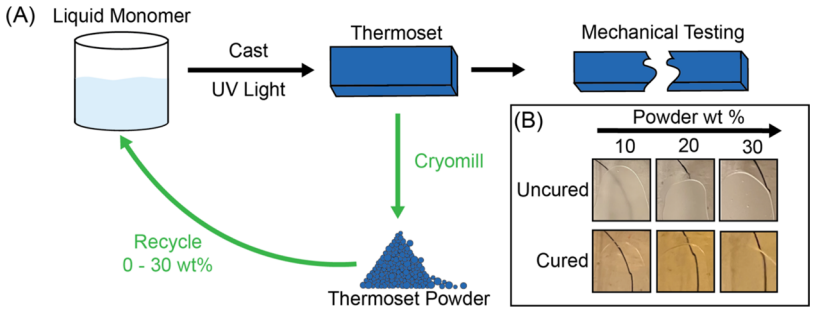

Figure 1. (A) Typical recycling and testing scheme indicating how a recycled material is added to the liquid resin during recycling. (B) Example of Formlabs Clear resin with recycled powder before and after curing with a black line behind to indicate transparency of the film.

film material. During the postcure process, a glass slide was placed on top to ensure that the tensile bars remained flat. The tensile bars were printed perpendicular to the build plate and designed to have a gauge length of 15 mm, a width of 3 mm, and a thickness of 1 mm.

3. CHARACTERIZATION

3.1. Tensile Testing. Tensile testing was conducted at room temperature with a Shimadzu Autograph AGS-X series instrument at 5 mm/min, using rubber grips for the model and clear resins. For elastic samples, the rate was increased to 50 mm/min, also using the rubber grips.

3.2. Dynamic Mechanical Analysis (DMA). DMA measurements were conducted using a TA Instruments RSA-G2 instrument with a rectangular tension geometry. A strain amplitude sweep was performed at a frequency of 1 Hz to determine the appropriate strain range to probe linear viscoelastic behavior. Temperature ramps were then conducted at 1 Hz with force tracking set to maintain an axial force that was at least 200% greater than the dynamic force with a minimum axial force of 3 g. The starting axial force depended on the sample type. For the clear resin sample, axial forces of 90 g were used because of the high sample stiffness, while for the elastic and model resins, only 30 g of axial force was applied to the sample. Auto strain adjustment was also enabled and set to 20% with a maximum strain of 1% and a minimum strain of 0.002%. For the clear resin, the samples were heated from 50 to 175 °C at a 5 °C/min rate under nitrogen gas. The sample was then cooled and heated again. The second heat is reported for all samples to remove any previous thermal history. For the elastic resin and the model resin samples, liquid nitrogen was used for cooling and as the inert gas source. The temperature range for the model resin was −20 to 70 °C and −60 to 50 °C for the elastic resin. For materials with a clear matrix and elastic particles or elastic matrix and clear particles, the temperature range was −50 to 150 °C to capture glass transition temperatures for both the clear and elastic resin.

3.3. Atomic Force Microscopy-Based Infrared Spectroscopy (AFM-IR). A Bruker NanoIR3 was used in "resonance enhanced" mode, where surface topography is tracked under Z feedback at constant cantilever deflection in contact mode, while IR laser light (MIRCAT 3-chip QCL, 904−1778 cm^{-1}, 10−20% power) is pulsed at the contact resonance frequency, which was tracked via phase-locked-loop (PLL) feedback. The amplitude of contact resonance oscillations due to photothermal expansion under pulsed IR irradiation gauges the strength of the IR absorption. Herein, we designate these images or mappings "IR absorbance". The variable contact resonance frequency (i.e., on different materials) qualitatively contrasts the normal stiffness of tip/sample contact (which is in series with the intrinsic cantilever stiffness, k) during imaging. Herein, we designate these images "AFM-IR stiffness". Eight data acquisition channels were employed, including height, deflection error signal, lateral force, and PLL error signal (lateral force and resonance amplitude being collected in both trace and retrace). Probes were of the Bruker PR-EX-NIR2 type (gold-coated tips to enhance IR field strength at the tip/sample interface) with a nominal spring constant of 0.07−0.4 N/m. The deflection set point was ∼10 to 15 nm (thus applied force ∼1 to 6 nN). Images were collected at a scanning frequency of 0.25 lines per second. Data sets were processed using the instrument's Analysis Studio software.

3.4. Optical Microscopy. An Olympus BX52 Microscope was used to image the particles by using a 4x objective. The particles were suspended in isopropyl alcohol and cast onto glass slides. After removal of the isopropyl alcohol, the particles were imaged. The red background color of the images is due to the microscope light source. A Zeiss EC EpiPlan optical microscope with a 5x objective and an AxioCam ICc 5 digital camera was used to image the layer thicknesses and resolution of the 3D-printed brick.

3.5. Particle Size Analysis. A Microtrac Bluewave laser diffraction analyzer and a Partan SIA image analyzer were used to analyze the clear resin particles and the size distribution. The particles were presuspended in DI water without any additional stabilizers prior to adding them to the flow system. The results are represented on a volume-weighted basis and reported as a mean particle size (M_v).

4. RESULTS AND DISCUSSION

4.1. Introduction to the Recycling Process. Vat photopolymerization 3D-printing produces parts with a layered morphology, which can substantially influence mechanical performance compared to bulk analogues. Therefore, the effects of recycled material in a cured thermoset without layers were first evaluated using the following workflow, also illustrated in Figure 1A: (1) Liquid resins (clear, elastic, and model) were cured between two glass slides to produce a thermoset film. (2) Thermoset films were cryomilled into a powder with average particle size of about 70 μm (details on powder size effects can be found in the SI). (3) The powder was mixed into the neat resins of interest at different target recycle contents and allowed to soak for 24 h. (4) The mixtures were cured, and the mechanical properties were evaluated through tensile testing.

4.2. Compositional Characteristics of Recycled Materials. For the two commercial resins, a translucent

https://doi.org/10.1021/acsapm.4c00184
ACS Appl. Polym. Mater. 2024, 6, 4625−4633

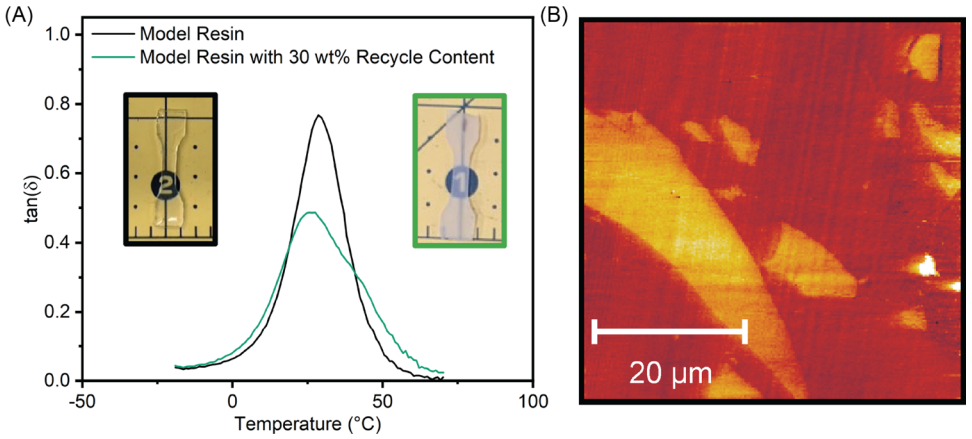

Figure 2. (A) Representative DMA tan(δ) data for cured samples as a function of temperature. The black data corresponds to the model resin (image on the left corresponds to the tensile bar, outlined in black). The green data corresponds to the model resin with 30 wt% recycle content (image on the right corresponds to the tensile bar, outlined in green). (B) AFM-IR stiffness image where brighter (yellow) areas correspond to stiffer regions and darker areas (red) correspond to softer regions.

mixture resulted when the cryomilled powder was recycled into the respective transparent liquid resin using the process described above. This observation is highlighted in the top row of the images in Figure 1B for the clear resin, where the sample obscures the view of the black line behind it. We hypothesize that this is due to slight refractive index differences between the cross-linked particles and liquid resin that causes light scattering. Once cured, both commercial materials with recycle content become fully transparent, as exemplified in the bottom row of images in Figure 1B for the clear resin where the black line is observable through the thermoset film containing up to 30 wt% recycle content. This suggests that the particles and the cured matrix have matching refractive indices.

To further investigate the integration of the particles with neat resin, macroscopic swelling studies were conducted. For these studies, a small piece of cured material was placed in liquid monomer, and the weight before and after 24 h of soaking was recorded; macroscopic diffusion time studies indicated that the mass uptake and mechanical properties plateau after 24 h. This is explained further in the SI and Figures S4−S6. As shown in Figure S7, the elastic network takes up 70 wt% elastic monomer resin, while the clear network takes up about 10 wt% clear monomer resin. This simple experiment confirms that the monomer diffuses readily into the preformed networks, which would be expected to facilitate physically interpenetrating networks from the recycled particles and the newly cured resin.

In contrast to the commercial resins, the model materials appeared translucent in the particle−resin mixtures and remained translucent postcure (postcure images shown as insets in Figure 2A). Recall that the model resin is a mixture of two different acrylates: isobornyl acrylate, a high T_g stiff material, and poly(ethylene glycol) diacrylate (PEG diacrylate), a low T_g soft material. A similar 24-h macroscopic swelling study was conducted on the model materials to understand diffusion of the different monomers into the cured powder particles. During this time frame, the cured material immersed in isobornyl acrylate takes up 1.9 ± 0.8 wt% monomer compared to 1.2 ± 0.3 wt% when immersed in PEG diacrylate (Figure S8). This suggests that isobornyl acrylate diffuses more rapidly into the recycled particles than PEG diacrylate, possibly due to the larger molecular size of the PEG diacrylate, which reduces mobility into the cross-linked particles. Intuitively, preferential swelling could promote compositional heterogeneity when a recycle material is incorporated, creating regions of different refractive indexes that scatter light once cured.

To further probe the compositional heterogeneity concept, DMA was employed to evaluate the sample moduli as a function of temperature. A relatively sharp symmetric tan(δ) peak is expected if the system is homogeneous, while a broad or multimodal tan(δ) peak is expected for a compositionally heterogeneous system.[21] The transparent model cured network (i.e., 0 wt% recycle content) displays a symmetric tan(δ) peak, as shown in Figure 2A, consistent with a uniform network. In contrast, the sample containing 30 wt% recycle content exhibited a high-temperature shoulder on the tan(δ) peak (Figures 2A and S9) indicative of a heterogeneous network. The higher temperature shoulder supports the diffusion studies and indicates that there are regions richer in isobornyl acrylate. In contrast, DMA on both elastic and clear resin materials shows a symmetric tan(δ) peak (Figures S10 and S11), suggesting that these materials are homogeneous, and there is no preferential monomer diffusion in the commercial materials, consistent with their clear appearance after curing.

To further probe the heterogeneity of the model materials, AFM-IR was used to examine the local chemical and mechanical characteristics of the cured samples. Results are shown in Figure 2B, where brighter regions correspond to stiffer regions, suggesting that the particles have a stiffness higher than that of the surrounding matrix. Both the DMA and monomer diffusion results are consistent with the hypothesis that isobornyl acrylate (rigid component) diffuses more rapidly into the recycled particles over PEG diacrylate (soft component). Upon UV exposure, isobornyl acrylate-rich monomers undergo photopolymerization within the cross-linked particles, creating an interpenetrating network richer in isobornyl acrylate making the particles stiffer. This is expected to change the refractive index of the particles compared to the surrounding matrix, consistent with observed light scattering and the translucent bulk appearance. Accordingly, IR mapping shows slight differences in the signal between the particles and the matrix, as shown in Figure S12, indicating detectable chemical differences between the two regions.

4.3. Mechanical Properties of Recycled Materials. Given the importance of mechanical properties in applications,

https://doi.org/10.1021/acsapm.4c00184
ACS Appl. Polym. Mater. 2024, 6, 4625−4633

tensile tests were conducted on both model and commercial materials with and without recycle content. A summary of these results for the model materials is shown in Figure 3 and

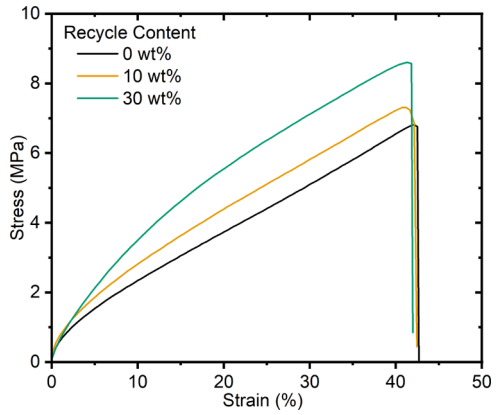

Figure 3. Representative stress−strain data for the model resin without (0 wt%) and with (10 and 30 wt%) recycle content.

Table S3. Model materials with up to 30 wt% recycle content could be easily processed, producing cured samples with a maximum stress of 8.19 ± 1.23 MPa and strain at break of 38.1 ± 5.5%, within error of the model material without recycle content (6.43 ± 0.59 MPa and 43.7 ± 5.4%).

A summary of the tensile test data for the commercial materials is shown in Table 1. The mechanical properties of the elastic commercial material drop slightly with 10 wt% recycle content. This is potentially due to the particles interfering with the strain-hardening mechanism during extension (Figure S13). Higher recycle contents were not investigated due to the significant increase in viscosity that occurred, which made it difficult to make films for testing. For the clear material, the mechanical properties do not change at 10 wt% recycle content. However, the strain at break, maximum stress, and toughness decreased at higher loadings.

A second recycling round was studied by taking a clear resin sample with 10 wt% recycle content and milling it to a powder. This second round of recycle powder has a similar average particle size to the first-cycle recycle material (Figure S2A,B). The second-round recycle powder was then reincorporated at 10 wt% into a neat liquid resin and cured. The maximum stress and strain at break for this material are within error of the original material (Table 1), suggesting that recycling can be performed multiple times while retaining the mechanical performance.

Considering all of the data presented to this point, our hypothesis for how the mechanical properties for recycled systems are maintained near that of cured neat materials is illustrated in Figure 4. Following diffusion of a liquid monomer

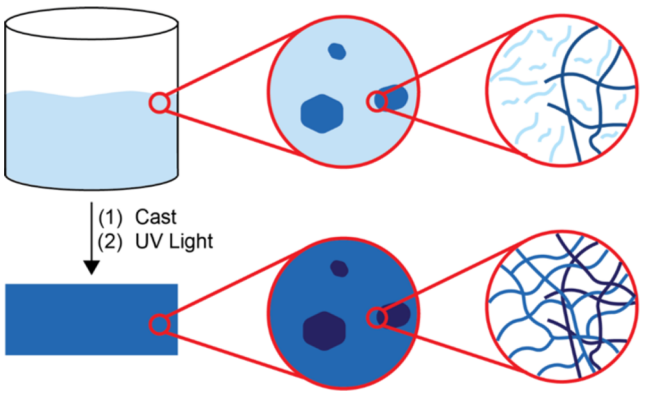

Figure 4. Illustration depicting the mechanism of diffusion and the formation of the interpenetrating network after exposure to UV light.

into cross-linked recycled particles, photopolymerization cures monomers inside and outside the particles. During photopolymerization, the original cross-linked particle network is physically integrated with the new cross-linked matrix that spans the entire system (inside and outside of the particles). Stress transfer between particles and the new network is facilitated by physical interlocking (or interpenetration) of the two networks, which also prevents particles from acting as mechanical failure sites.

4.4. Recycling Mixed Materials. While monomaterial recycling is attractive by analogy to regrind for thermoplastics, real recycling streams are typically more diverse. For example, mixed plastic waste streams are a common occurrence for mechanical recycling of thermoplastics, and this typically leads to a significant decrease in the mechanical properties of these materials due to immiscibility.[22] Therefore, mixed thermoset waste streams are also likely to be commonplace and should be examined in the mechanical recycling process.

The mechanism described at the end of the last section suggests that mechanically robust, recycled materials should be attainable as long as the fresh monomer is able to diffuse into the network of a given recycle particle type. To further investigate this hypothesis, cryomilled clear powder particles were mixed into an elastic liquid resin, and vice versa, following the procedure described in Figure 1A. The mechanical and

Table 1. Tensile Test Results as a Function of Recycle Content and Resin Type

recycle content (wt%)	strain at break (%)	max stress (MPa)	modulus (GPa)	toughness (MJ/m^3)	number of samples
Resin Material: Clear | Recycle Content: Clear					
0	13.5 ± 2.9	76.4 ± 3.2	1.13 ± 0.08	7.10 ± 2.00	13
10	12.2 ± 2.9	72.5* ± 5.0	1.11 ± 0.11	5.91 ± 1.98	16
10 (2nd round)	10.6 ± 2.2	74.8 ± 1.9	1.22* ± 0.07	5.06* ± 1.59	6
20	10.4* ± 1.9	68.6* ± 3.7	1.13 ± 0.05	4.50* ± 1.18	5
30	8.9* ± 1.5	66.0* ± 9.1	1.11 ± 0.10	3.61* ± 1.13	3
Resin Material: Elastic | Recycle Content: Elastic					
0	285 ± 23	4.57 ± 1.16	0.0018 ± 0.0001	5.23 ± 1.25	8
10	235* ± 10	3.00* ± 0.28	0.0018 ± 0.0001	3.36* ± 0.32	5

*Indicates that the data point is statistically significant from the two-sample t test with a significance value of 0.05 compared to the original material with no recycle content.

https://doi.org/10.1021/acsapm.4c00184
ACS Appl. Polym. Mater. 2024, 6, 4625−4633

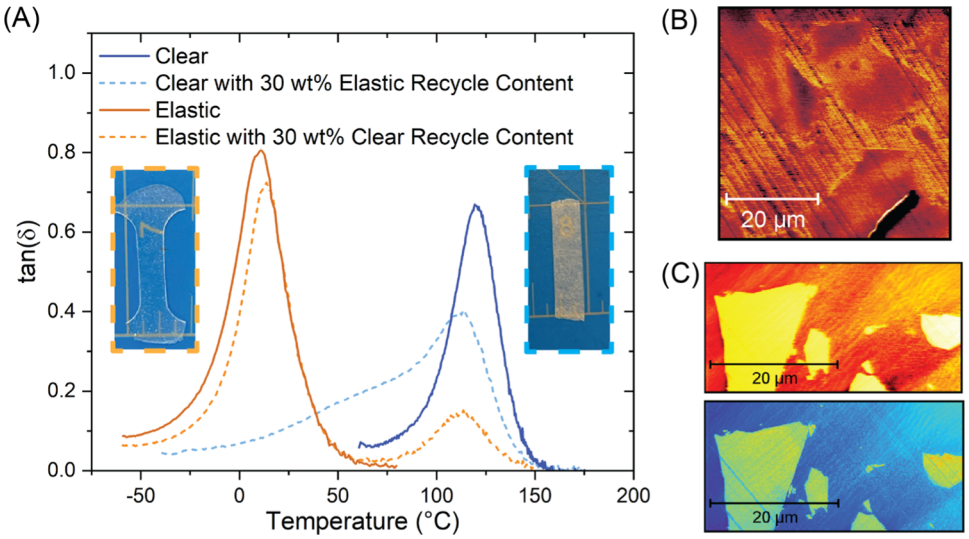

Figure 5. (A) tan(δ) vs temperature second heating data for networks made up of clear, elastic, clear with 30 wt% elastic recycle content (image of corresponding tensile bar on the right outlined in blue), and elastic with 30 wt% clear recycle content (image of corresponding tensile bar on the left outlined in orange). (B) AFM-IR stiffness mapping of clear with 30 wt% elastic recycle content. (C) AFM-IR stiffness mapping (top) and IR absorbance mapping at 1142 cm^{-1} (bottom) of elastic with 30 wt% clear recycle content.

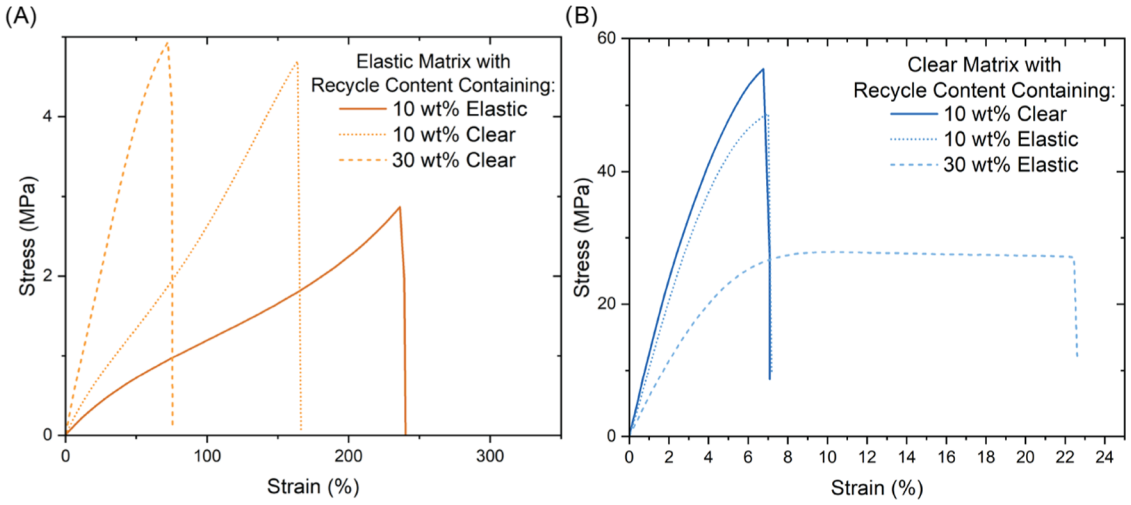

Figure 6. Representative stress−strain data for cured samples comprising (A) an elastic matrix with 10 wt% elastic, 10 wt% clear, or 30 wt% clear recycle content and (B) a clear matrix with 10 wt% clear, 10 wt% elastic, or 30 wt% elastic recycle content.

rheological properties, as well as the microstructure of the resulting materials were analyzed.

Unsurprisingly, these networks are translucent both after mixing and after curing (images of materials after curing shown in Figure 5A) due to chemical differences between the elastic and clear resins, causing differences in the refractive indices. AFM-IR was used to examine the chemical and physical differences between the particles and the matrix. In Figure 5B, the stiffness map of the clear matrix with 30 wt% elastic recycle content demonstrates recycled particles that are slightly softer than the surrounding matrix. However, the distinction in modulus between the matrix and the particles is not as stark in these mixtures, suggesting that the elastic recycled particles are absorbing significant amounts of the liquid clear resin to create an interpenetrating network with a more homogeneous modulus. IR mapping of this material does not show distinct signals regarding a heterogeneous chemical composition (Figure S14) between the matrix and the particles. To further probe if significant monomer diffusion is occurring in this system, macroscopic diffusion studies and DMA were used. Macroscopic diffusion studies indicated that an elastic matrix immersed in clear liquid resin absorbs about 25 wt% of the clear monomer (Figure S7). DMA results in Figure 5A support these observations where the clear network with 30 wt% elastic recycle content has a broad bimodal peak that spans the entire range of glass transition temperatures between the neat clear and neat elastic material. Together, this indicates significant monomer swelling of the elastic particles with clear resin and supports the likelihood of an interpenetrating network after UV curing.

In contrast, for the elastic matrix with 30 wt% clear recycle content, the stiffness map from AFM-IR shown in the top image in Figure 5C demonstrates that the particles have a much higher modulus than the surrounding matrix. This suggests that there may be less monomer diffusion in this system, leading to more significant chemical differences that can be evaluated via AFM-IR. A diagnostic peak can be assigned for the clear resin at 1142 cm^{-1}, which is missing for

https://doi.org/10.1021/acsapm.4c00184
ACS Appl. Polym. Mater. 2024, 6, 4625−4633

Table 2. Tensile Test Data for 3D-Printed Tensile Bars Printed at a 200 μm Layer Thickness and Post Curing for 15 min

recycle content (wt%) (average particle diameter)	strain at break (%)	max stress (MPa)	modulus (GPa)	toughness (MJ/m^3)	number of samples
0	13.4 ± 1.8	52.0 ± 1.7	0.83 ± 0.05	5.05 ± 0.86	6
10 (70 μm)	11.6 ± 2.3	46.7 ± 6.2	0.70* ± 0.08	4.19 ± 0.41	6
10 (122 μm)	9.4* ± 1.4	43.3* ± 0.7	0.67* ± 0.04	2.54* ± 0.62	5

*Indicates that the data point is statistically significant from two-sample t test with a significance value of 0.05 compared to the original material with no recycle content.

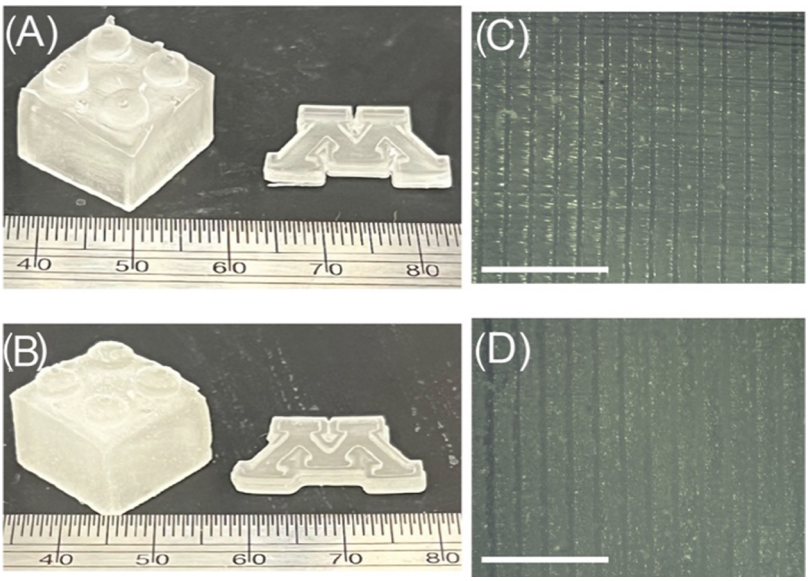

Figure 7. Images of a 3D-printed clear resin brick and "M" with (A) 0 wt% recycle content and (B) 10 wt% recycle content. Optical microscope images with scale bars of 1 mm of the layers on a side of a 3D-printed clear resin brick with (C) 0 wt% recycle content and (D) 10 wt% recycle content.

the elastic resin (Figure S15). IR mapping at 1142 cm^{-1}, as shown in Figure 5C, indicates distinct chemical differences between the particles and the surrounding matrix. However, it is not evident from AFM-IR that the monomer diffusion mechanism is present in this system. DMA and macroscopic swelling studies can be used to take a closer look at the monomer diffusion mechanism. DMA results in Figure 5A for the elastic matrix with 30 wt% clear recycle content demonstrate distinct glass transition temperatures close to the original materials. However, the glass transition temperatures of the mixed system shift slightly from those of the neat materials, indicating a small amount of monomer diffusion occurring in these samples. Macroscopic swelling studies corroborate these results where a clear matrix immersed in elastic liquid resin for 24 h takes up ∼2 wt% elastic monomer (Figure S7).

To confirm the formation of a mechanically robust interpenetrating network, tensile tests were conducted and the results are summarized in Table S4 with representative stress−strain data shown in Figure 6. At low recycle content loadings (10 wt%), it was demonstrated that the particle identity does not influence the toughness of the materials. In other words, the 10 wt% elastic recycle content in an elastic matrix has a toughness similar to the 10 wt% clear recycle content in an elastic matrix. Overall, this indicates that at low recycle content, contaminates in the recycle stream may have little effect on the mechanical properties of the system. However, when the recycle content was increased to 30 wt%, the recycled particles either embrittled (Figure 6A) or toughened (Figure 6B) the matrix depending on the material choice. These findings are similar to those observed in rubber-toughened epoxies,[23−25] where a low T_g elastic particle in a glassy matrix results in a more ductile material (Figure 6B). In total, these data suggest that as long as the recycled networks can absorb even small amounts of monomer, the resulting interpenetrating network will prevent particles from acting as failure sites and enable the recycling of even mixed materials.

4.5. SLA 3D-Printing. Finally, to demonstrate this recycling approach in commercial 3D-printing applications, the Formlabs clear resin with 0 and 10 wt% recycle content was utilized for a 3D-printing study using a Formlabs Form 1+ printer. A loading of 10 wt% recycle content was selected because its mechanical properties were consistent with neat, cured resins in the previous film studies (Table 1). Table 2 summarizes tensile testing results from tensile specimens printed perpendicular to the build plate. These results indicate that adding 10 wt% recycle content does not significantly affect the mechanical properties of the printed parts. However, similar to the film studies (discussion included in the SI), the particle size of the recycled material is important. When the clear resin is milled to an average diameter of 70 μm (Figure S2C), like in the film studies (see discussion in the SI), the mechanical properties are not significantly different from the neat material. However, when the clear resin is only milled, two cycles produce an average particle diameter of 122 μm (Figure S2D), the mechanical properties are significantly reduced, as shown in Table 2. We hypothesize this is due to larger particles causing defects and reducing adhesion between printed layers, which is more likely as the particle size becomes closer to the print layer thickness, here 200 μm.

https://doi.org/10.1021/acsapm.4c00184
ACS Appl. Polym. Mater. 2024, 6, 4625−4633

In addition to the mechanical properties of the 3D-printed parts, the layer resolution as a function of particle amount and size was also investigated. Two objects were printed to observe opacity and layer resolution differences (Figure 7A,B; 70 μm particle size). Visually, the materials with recycle content appear to have approximately the same opacity as those without recycle content. However, it should be noted that these 3D-printed parts with and without recycle content are more opaque than the single-layer materials shown in Figure 1 due to trapped air bubbles or other defects, within and between the layers, that scatter light. The layers for parts with the recycle material added have a slight surface roughness (Figure 7D) compared to samples without recycle content (Figure 7C).

For many 3D-printed structures, parts are printed at a slight angle from the build plate using support structures. This tends to create parts with the least number of defects during the print and prevents them from adhering to the resin tray. Therefore, the bricks were printed on an angle with support structures, as can be seen in Figure S16. Two bricks were printed at slightly different angles to ensure print success, with one printed at a much more severe angle than the other. Surprisingly, the angle of the printed part has a considerable effect on the resolution of these layers when recycled material is incorporated; without recycled materials, the angle does not appear to matter, and layers are clearly visible on all sides of the brick (Figure S17). As the sides of the brick become more perpendicular to the print surface, the surface becomes smoother when the particle size of the recycle content is 70 μm (Figure S18) versus 122 μm (Figure S19). This difference is potentially due to the smaller recycled particles scattering/diffracting more light, as there is a higher number density of particles for the same weight percentage recycle content. Additionally, the scattering angles from smaller particles are expected to be larger, making the light more diffuse/less focused.[26,27] It is also important to appreciate that the irregular surfaces of the particles can also contribute to light scattering/diffraction, and it is unclear how different these structures may be between the different particle size recyclates. Regardless, it is intuitive that these combined factors could reduce the achievable resolution by scanning lasers during printing. The same phenomenon is seen when 50 μm layers are printed, where the sample with recycled particles milled to 70 μm has less layer definition than the other two materials, resulting in a surface that is smooth and appears to have no layers present (Figures S20−S22). This effect could be advantageous if the layer lines interfere with the aesthetics of the print. Currently, postprinting techniques, such as sanding with sandpaper, are used to remove layer lines and smooth the overall appearance of 3D-printed parts. With the recycled material, this postprinting modification might be unnecessary to achieve a smooth part.

4.6. Conclusions. In summary, we have demonstrated that mechanical recycling of UV-curable thermosetting resins is an effective method of reducing 3D-printed plastic waste. It was determined that at least 10 wt% of the mechanically recycled thermoset resin can be recycled back into the uncured liquid resin with minimal loss in mechanical properties. Mechanical recycling was performed with an in-house resin as well as two commercially available resins. DMA and AFM-IR studies revealed that the mechanical properties of materials with recycle content could be maintained due to the monomers diffusing into the recycled particles. Upon UV exposure, the monomers polymerize to create an interpenetrating network, preventing the particles from acting as mechanical failure sites. Due to this monomer diffusion process, the visual properties of the materials can be tuned by a judicious choice of monomer. Additionally, mixed recycled materials were investigated to mimic a real recycling stream. It was determined that with low loadings of a recycle contaminate (10 wt%), the toughness of the original material can be maintained. However, it was also demonstrated that adding high loadings (30 wt%) of a recycle contaminate could be leveraged to change the mechanical properties of the original material. Finally, a commercial material with 10 wt% recycle content was 3D-printed, demonstrating that the mechanical and visual properties of these printed parts are maintained. Overall, these results will allow for more efficient recycling of photopolymerized 3D-printed thermosets without the need for postprocessing or resin modifications.

■ ASSOCIATED CONTENT

Supporting Information

The Supporting Information is available free of charge at https://pubs.acs.org/doi/10.1021/acsapm.4c00184.

Discussion and tensile data on batch-to-batch variations; discussion on particle size effects with microscope images, particle size analysis, and tensile data; discussion on monomer diffusion with swelling data, tensile data, rheology data, and AFM-IR; supporting tensile data for materials containing recycle content; 3D-printing set up; and microscopic images of 3D-printed parts (PDF)

■ AUTHOR INFORMATION

Corresponding Authors

Theresa M. Reineke − *Department of Chemistry, University of Minnesota, Minneapolis, Minnesota 55455, United States;* orcid.org/0000-0001-7020-3450; Email: treineke@umn.edu

Christopher J. Ellison − *Department of Chemical Engineering and Materials Science, University of Minnesota, Minneapolis, Minnesota 55455, United States;* orcid.org/0000-0002-0393-2941; Email: cellison@umn.edu

Authors

Erin M. Maines − *Department of Chemical Engineering and Materials Science, University of Minnesota, Minneapolis, Minnesota 55455, United States;* orcid.org/0009-0002-8416-6333

Michaela A. Polley − *Department of Chemistry and Department of Mathematics and Statistics, Carleton College, Northfield, Minnesota 55057, United States*

Greg Haugstad − *Characterization Facility, University of Minnesota, Minneapolis, Minnesota 55455, United States*

Brenda Zhao − *Department of Chemical Engineering and Materials Science, University of Minnesota, Minneapolis, Minnesota 55455, United States*

Complete contact information is available at: https://pubs.acs.org/10.1021/acsapm.4c00184

Notes

The authors declare no competing financial interest.

■ ACKNOWLEDGMENTS

The authors would like to thank Fang Zhou for the sample preparation of cryomicrotomed samples on the model and

elastic materials, as the elastic samples were particularly difficult due to their low glass transition temperature. They would like to thank Dr. James Marti for particle size analysis of the resin powder. They would also like to thank Rui Ding for developing the STL file to print the "M" and the instructors for the brick STL file used, which was created for the undergraduate materials science and engineering laboratory course at the University of Minnesota. Additionally, they would like to thank the following people who the took time to review early drafts of this manuscript and contributed to figure design: Dr. Mayuri Porwal, Dr. Jeffrey Self, Dr. Aristotelis Zografos, and Dr. Emily McGuinness. The authors acknowledge the funding sources for this work: the National Science Foundation Center for Sustainable Polymers at the University of Minnesota, which is a National Science Foundation supported Center for Chemical Innovation (CHE-1901635), and the National Science Foundation Graduate Research Fellowship Program (Grant No. 1839286). Any opinions, findings, and conclusions expressed in this work are those of the authors and do not necessarily reflect the views of the National Science Foundation. Parts of this work were carried out in the Characterization Facility at the University of Minnesota, which receives partial support from the NSF through the MRSEC (Award Number DMR-2011401) and the NNCI (Award Number ECCS-2025124) programs. Particle size analysis was conducted in the Minnesota Nano Center, which is supported by the National Science Foundation through the National Nanotechnology Coordinated Infrastructure (NNCI) under Award Number ECCS-2025124.

REFERENCES

(1) Karevska, S.; Steinberg, G.; Müller, A.; Wienken, R.; Kilger, C.; Krauss, D. 3D Printing: Hype or Game Changer?. https://assets.ey.com/content/dam/ey-sites/ey-com/en_gl/topics/advisory/ey-3d-printing-game-changer.pdf (accessed Oct 21, 2020).

(2) Stewart, D. Technology, Media, and Telecommunications Predictions 2019:3D Printing Growth Accelerates Again. https://www2.deloitte.com/content/dam/insights/us/articles/TMT-Predictions_2019/DI_TMT-predictions_2019.pdf (accessed Oct 5, 2020).

(3) Geyer, R. Production, Use, and Fate of Synthetic Polymers. In *Plastic Waste and Recycling*; Letcher, T. M., Ed.; Elsevier, 2020; pp 13−32.

(4) Pakkanen, J.; Manfredi, D.; Minetola, P.; Iuliano, L. About the Use of Recycled or Biodegradable Filaments for Sustainability of 3D Printing. *Smart Innov. Syst. Technol.* **2017**, *68*, 776−785.

(5) Shanmugam, V.; Das, O.; Neisiany, R. E.; Babu, K.; Singh, S.; Hedenqvist, M. S.; Berto, F.; Ramakrishna, S. Polymer Recycling in Additive Manufacturing: An Opportunity for the Circular Economy. *Mater. Circ. Econ.* **2020**, *2* (1), 11.

(6) Maines, E. M.; Porwal, M. K.; Ellison, C. J.; Reineke, T. M. Sustainable Advances in SLA/DLP 3D Printing Materials and Processes. *Green Chem.* **2021**, *23* (18), 6863−6897.

(7) Morici, E.; Dintcheva, N. T. Recycling of Thermoset Materials and Thermoset-Based Composites: Challenge and Opportunity. *Polymers* **2022**, *14* (19), 4153.

(8) Voet, V. S. D.; Guit, J.; Loos, K. Sustainable Photopolymers in 3D Printing: A Review on Biobased, Biodegradable, and Recyclable Alternatives. *Macromol. Rapid Commun.* **2021**, *42* (3), 1−11.

(9) Zhu, G.; Houck, H. A.; Spiegel, C. A.; Selhuber-Unkel, C.; Hou, Y.; Blasco, E. Introducing Dynamic Bonds in Light-based 3D Printing. *Adv. Funct. Mater.* **2023**, 2300456 DOI: 10.1002/adfm.202300456.

(10) Fei, M.; Liu, T.; Zhao, B.; Otero, A.; Chang, Y. C.; Zhang, J. From Glassy Plastic to Ductile Elastomer: Vegetable Oil-Based UV-Curable Vitrimers and Their Potential Use in 3D Printing. *ACS Appl. Polym. Mater.* **2021**, *3* (5), 2470−2479.

(11) Zhang, B.; Kowsari, K.; Serjouei, A.; Dunn, M. L.; Ge, Q. Reprocessable Thermosets for Sustainable Three-Dimensional Printing. *Nat. Commun.* **2018**, *9* (1), 1831.

(12) Gao, H.; Sun, Y.; Wang, M.; Wang, Z.; Han, G.; Jin, L.; Lin, P.; Xia, Y.; Zhang, K. Mechanically Robust and Reprocessable Acrylate Vitrimers with Hydrogen-Bond-Integrated Networks for Photo-3D Printing. *ACS Appl. Mater. Interfaces* **2021**, *13* (1), 1581−1591.

(13) Chen, Z.; Yang, M.; Ji, M.; Kuang, X.; Qi, H. J.; Wang, T. Recyclable Thermosetting Polymers for Digital Light Processing 3D Printing. *Mater. Des.* **2021**, *197*, 109189.

(14) Li, A.; Challapalli, A.; Li, G. 4D Printing of Recyclable Lightweight Architectures Using High Recovery Stress Shape Memory Polymer. *Sci. Rep.* **2019**, *9* (1), 7621.

(15) Podgórski, M.; Huang, S.; Bowman, C. N. Additive Manufacture of Dynamic Thiol−Ene Networks Incorporating Anhydride-Derived Reversible Thioester Links. *ACS Appl. Mater. Interfaces* **2021**, *13*, 12789−12796, DOI: 10.1021/acsami.0c18979.

(16) Li, X.; Yu, R.; He, Y.; Zhang, Y.; Yang, X.; Zhao, X.; Huang, W. Four-Dimensional Printing of Shape Memory Polyurethanes with High Strength and Recyclability Based on Diels-Alder Chemistry. *Polymer* **2020**, *200*, 122532.

(17) Poelma, J.; Rolland, J. P.; Curvers, R. H. N.; Desimone, J. M. Reversible Thermosets for Additive Manufacturing. US Patent US11,135,7442021.

(18) Jia, Y.; Ling, F.; Qian, J.; Chen, Q.; Zhao, Z.; Li, Y. Fast Damage-Healing of Rigid Photocuring 3D Printing Materials Capable of Directly Recycling in 3D Printing. *ACS Macro Lett.* **2023**, *12* (6), 719−724.

(19) Zhu, G.; Zhang, J.; Huang, J.; Qiu, Y.; Liu, M.; Yu, J.; Liu, C.; Shang, Q.; Hu, Y.; Hu, L.; Zhou, Y. Recyclable and Reprintable Biobased Photopolymers for Digital Light Processing 3D Printing. *Chem. Eng. J.* **2023**, *452* (P3), 139401.

(20) Li, H.; Zhang, B.; Wang, R.; Yang, X.; He, X.; Ye, H.; Cheng, J.; Yuan, C.; Zhang, Y.; Ge, Q. Solvent-Free Upcycling Vitrimers through Digital Light Processing-Based 3D Printing and Bond Exchange Reaction. *Adv. Funct. Mater.* **2022**, *32* (28), 1−11, DOI: 10.1002/adfm.202111030.

(21) Yang, J.; Winnik, M. A.; Ylitalo, D.; DeVoe, R. J. Polyurethane−Polyacrylate Interpenetrating Networks. 1. Preparation and Morphology. *Macromolecules* **1996**, *29* (22), 7047−7054.

(22) Higgins, J. S.; Lipson, J. E. G.; White, R. P. A Simple Approach to Polymer Mixture Miscibility. *Philos. Trans. R. Soc., A* **2010**, *368* (1914), 1009−1025.

(23) Pearson, R. A. Toughening Epoxies Using Rigid Thermoplastic Particles. 1993, 405−425.

(24) Huang, Y.; Hunston, D. L.; Kinloch, A. J.; Riew, C. K. Mechanisms of Toughening Thermoset Resins. 1993, 1−35.

(25) Bagheri, R.; Marouf, B. T.; Pearson, R. A. Rubber-Toughened Epoxies: A Critical Review. *Polym. Rev.* **2009**, *49* (3), 201−225.

(26) Xu, R. *Particle Characterization: Light Scattering Methods*; Kluwer Academic Publishers, 2002.

(27) Vargas-Ubera, J.; Gale, D. M.; Felix-Aguilar, J. The Rage of Validity of the Fraunhofer Approximation in the Estimation of Particle Size Distributions from Light Diffraction. *Proc. SPIE* **2001**, *4419*, 435−438.